DETECTING CURVES IN VERY NOISY IMAGES USING FOURIER-ARGAND MOMENTS

Tianle Zhao and Thierry Blu

Department of Electronic Engineering, The Chinese University of Hong Kong, Hong Kong

ABSTRACT

Detection of curves (e.g., ridges) from very noisy images is an important yet challenging task in photon-starved imaging applications (e.g., nuclear imaging modalities, fluorescence/electron microscopy, radioastronomy, first photon/light-in-flight imaging).

In this paper, we exploit the consistency of the image along the curve, i.e., the fact that the image changes slowly when we move along the curve—"locally" laminar images. We compute a sequence of complex scalars that we call Fourier-Argand moments, and show that the direction of variation of a laminar image is purely encoded in the phase of these moments. In particular, focusing on ridges located at the center of the image, we show that using these moments altogether in a frequency estimation algorithm provides a very accurate and highly robust estimate of the direction of the ridge: we demonstrate this accuracy for noise levels as high as $-10\,$dB.

We then show how to detect curves—i.e., local ridges—by computing the Fourier Argand moments within a sliding window across the image, and design a consistency map whose thresholding allows to keep only the pixels on the curve.

Numerical experiments on both synthetic images and real images (low light photography) demonstrate the accuracy and robustness to noise of the proposed method, compared to a state of the art method.

Index Terms— Laminar image, directional feature, rotation covariant moments, frequency estimation, curve detection.

1. INTRODUCTION

The ability to recover images from very noisy measurements has always been crucial to many research areas ranging from physics to biology. In particular, starved-photon techniques are now used for 3D image reconstruction [1] and non line-of-sight imaging [2]. In these applications, the very low photon flux makes the noise due to photon counting particularly high.

Confocal fluorescence microscopy is another instance of very low intensity light measurements, caused by, both the weak fluorescence process, and the existence of a pinhole which discards most of this light to achieve optical sectioning. In this case, to obtain visually plausible images, long exposure times (seconds) are usually required, which hinder the observation of faster dynamic processes. Techniques that are able to retrieve signals buried in large noise should in principle reduce the exposure time and hence enable the observation of dynamic processes. Indeed, ridge and edge detection is a fundamental task for many applications in the field of image processing, such as image segmentation [3, 4], content analysis [5, 6] and detection [7], etc.

In the derivation of his classical edge detection algorithm, Canny [8] used the first derivatives of a Gaussian to approximate the optimal edge filter. The gradients of an image computed using the filters are then used to detect edges and to estimate their directions. Later on, starting from the perspective of matched filtering, Jacob et. al. [9] proposed to approximate the matched filter in the family of steerable filters. They also reformulated Canny's filter (together with his optimality criteria) in this steerable filter framework. The key idea of the approximation is that, by assuming a filter to be a linear combination of several basis filters (derivatives of an isotropic window function) rotating the filter amounts to changing the coefficients of the linear combination without changing the basis filters. This solves the problem for matched filtering that when higher directional accuracy is required, the number of rotations needed for the filter quickly becomes too large. Lindeberg addressed the problem of selecting the intrinsic scales of ridges in [10], while at each scale he still used the second order derivatives of an isotropic Gaussian function.

A common problem of above algorithms is that the estimation of the direction is not accurate enough due to the low directional sensitivity of the filters. In this paper, we show how to approach the problem from a different perspective, by exploiting the local directional consistency of curve images. For this, we will first consider ideally consistent images: laminar images; i.e., images that varies only in one direction θ,

$$I(x,y) = f(x\cos\theta + y\sin\theta), \qquad (1)$$

for some real-valued "shape" function $f(x)$ and a direction $\theta \in [0, 2\pi)$. This general formulation includes ridges, i.e., *symmetric* and localised shape function (typically, a Gaussian); and edges, i.e., *anti-symmetric* shape function (typically, a sigmoid), plus to a constant.

We propose to compute complex-valued quantities that
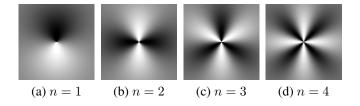
(a) $n = 1$ (b) $n = 2$ (c) $n = 3$ (d) $n = 4$

Fig. 1. Real parts of the complex-valued filters used for computing the Fourier-Argand moments for different n.

we call Fourier-Argand moments[1]. For laminar images, we show that the direction θ is solely encoded in the phase of the moments. The good properties of the proposed Fourier-Argand moments are actually related to the concept of rotation covariance studied in [13, 14]. More importantly, using several of these moments together, we are able to estimate the direction θ of centered ridges with very high accuracy, even when the image is buried in heavy noise.

Localizing this algorithm by computing the Fourier-Argand moments within a sliding window across the image, allows us to use this algorithm to estimate the local direction of the curve. In order to distinguish between curve and non-curve pixels in the image, we devise a consistency map which, after adequate thresholding, provides the curve pixel location—and the accurate local curve direction.

2. ROTATIONAL MOMENTS OF LAMINAR IMAGES

In this section, we assume the image $I(x, y)$ to be laminar and show how its direction of variation can be estimated from the phase of Fourier-Argand moments.

2.1. Fourier-Argand moments

We propose to compute the following moments of an image $I(x, y)$ defined for all positive integers n.

$$M_n = \iint I(x, y) \left(\frac{x + iy}{|x + iy|} \right)^n w(|x + iy|) \, \mathrm{d}x\mathrm{d}y, \quad (2)$$

where $i^2 = -1$ and the (positive) window function w is typically a Gaussian function: $w(r) = \exp\left(-r^2/(2\sigma^2)\right)$, where σ is the size of this window. We name these moments as Fourier-Argand moments because of their rotational covariance (Argand) and their frequency interpretation (Fourier). Fig. 1 shows the filters corresponding to the moments for different n. Pure black means -1 and pure white means 1.

Let the image be laminar, i.e., $I(x, y)$ varies only in the direction θ according to (1). Substituting (1) into (2) and by

the change of variable $x + iy = \mathrm{e}^{i\theta}(x' + iy')$, we find

$$M_n = a_n \, \mathrm{e}^{in\theta}, \quad (3)$$

where $a_n = \iint f(x) \left(\frac{x + iy}{|x + iy|} \right)^n w(|x + iy|) \, \mathrm{d}x\mathrm{d}y.$ (4)

Notice that a_n is real for any real-valued f and integer n, because a change of variable $y' = -y$ shows that a_n equals its complex conjugate. Therefore, the direction θ is purely encoded in the phase of the moments.

2.2. Centered ridge moments

Ridges are laminar images for which the shape function $f(x)$ is symmetric, and localized—e.g., a Gaussian function. When the symmetry is around $x = 0$, i.e., when the ridge is centered, then it is easy to check from (4) that all the odd degree moments vanish:

$$f(x) = f(-x) \implies M_{2n-1} = 0, n = 1, 2, \ldots. \quad (5)$$

Moreover, we notice that, for a centered ridge, the signs of a_{2n} usually alternate; i.e., $\mathrm{sign}(a_{2n}) = -\mathrm{sign}(a_{2n+2})$, for $n \geq 0$. To see this, let us compute the even-order Fourier-Argand moments for a Dirac that varies in direction θ. Substituting $I(x, y) = \delta(x \cos \theta + y \sin \theta)$ into (2) and changing to polar coordinates, we have

$$
\begin{aligned}
M_{2n} &= \int_0^\infty r w(r) \, \mathrm{d}r \int_0^{2\pi} \delta(r \cos(\alpha - \theta)) \mathrm{e}^{i2n\alpha} \, \mathrm{d}\alpha \\
&= \underbrace{(-1)^n \mathrm{e}^{i2n\theta}}_{\exp(in(2\theta + \pi))} \times \underbrace{2 \int_0^\infty w(r) \, \mathrm{d}r}_{> 0}
\end{aligned}
\quad (6)
$$

Hence, a property of a centered ridge is that its *normalized* Fourier-Argand moments $M_{2n}/|M_{2n}|$ follow a pure complex exponential model $\exp(in\alpha)$, where $\alpha = 2\theta + \pi$.

2.3. Centered ridge direction estimation

We have just shown that the direction of a centered ridge is encoded only in the phase of the *even* Fourier-Argand moments—not in their amplitude. Although any of these moments can, individually, provide the direction information (up to a multiple of π/n), their lack of directional sensitivity make them very inaccurate in practical situations. Fortunately, using several of these moments altogether increases this accuracy dramatically, as we show in the following.

Assume that we have computed the first N even-order Fourier-Argand moments of a centered ridge: M_{2n}, $n = 1, 2, \ldots, N$. Estimating θ can be done by minimizing the difference between the sequence of complex numbers $M_{2n}/|M_{2n}|$ and the model $\exp(in\alpha)$ that is suggested by (6); or, if we choose least-squares minimization, by computing

$$\alpha^* = \arg \max_{\alpha \in [0, 2\pi)} \mathrm{Re}\left(\sum_{n=1}^{N} \frac{M_{2n}}{|M_{2n}|} \mathrm{e}^{-in\alpha} \right). \quad (7)$$

---

[1] Jean-Robert Argand is credited for the geometric interpretation of complex numbers $x + iy$ at the beginning of the XIX century [11]. See [12] for a geometric link between the Fourier transform and the Argand interpretation.
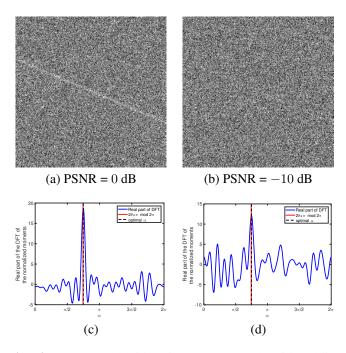
(a) PSNR = 0 dB   (b) PSNR = −10 dB

(c)   (d)

Fig. 2. Centered ridge image corrupted with additive Gaussian noise of PSNR $0\,$dB (a) and $-10\,$dB (b). The DFT of the normalized Fourier-Argand moments, $\left\{ M_{2n}/|M_{2n}| \right\}_{n=1,2,\ldots,20}$, of the images in (a) and (b) is computed, and their real part shown in (c) and (d). The maximum of these graphs matches the ground-truth direction of the ridge very closely, despite the very high noise level.

According to our findings in Subsection 2.2, the least-squares optimal α^* is related to an estimate of θ by

$$\hat{\theta} = \frac{\alpha^* - \pi}{2} \mod \pi, \qquad (8)$$

Note that the π-uncertainty is of no consequence here (direction of a line).

The solution of (7) can be found either exactly, by solving for the roots of a polynomial of degree $2N$, or approximately, by maximizing the real part of a Discrete Fourier Transform over 360 points. The DFT choice provides an angle accuracy of $0.5°$, which is sufficient in practice.

Fig. 2 demonstrates the very high robustness and directional sensitivity of the estimator (7). Here, 20 moments are computed from a centered ridge image corrupted at different noise levels. Both at $0\,$dB and at $-10\,$dB, the real-part of the DFT of these normalized moments has a sharp maximum close to the ground truth $\alpha = 2\theta + \pi \mod 2\pi$. We should mention that this high sensitivity comes from the fact that estimating frequencies is actually much more accurate than estimating amplitudes (see [15]).

3. A CURVE DETECTION ALGORITHM

In Section 2, we proposed an algorithm for estimating the direction of centered ridges. We now want to show how this al-

gorithm can be applied to non-centered ridges, and more generally, to curves. The principle is that, within a small window, a "consistent" curve (avoiding sharp turns) can be approximated reasonably well by a ridge, and that if the window is located adequately, this ridge is centered.

3.1. Fourier-Argand filters and curve direction

Since the Fourier-Argand moments are already localized using the window $w(|x+iy|)$, we can just shift the image $I(x,y)$ at various positions to obtain localized Fourier-Argand moments across the image. Accordingly, this transforms the integral definition (2) of the moments into a convolution. Specifically, consider the filters defined by

$$h_n(x,y) = \left(-\frac{x+iy}{|x+iy|} \right)^n w(|x+iy|),$$

then the localized Fourier-Argand moments result from the 2D convolution $M_n(x,y) = (I * h_n)(x,y)$.

Once these moments have been computed at every point of the image, we can use the frequency estimation algorithm (7) discussed in Section 2.3. This provides us with an image $\alpha^*(x,y)$ that is related to an image of pointwise direction estimates $\hat{\theta}(x,y) = \left(\alpha^*(x,y) - \pi \right)/2 \mod \pi$.

3.2. Reliability criterion

What we have found in Section 2.3 is that the direction estimate $\hat{\theta}(x,y)$ at (x,y) is very accurate, even in the presence of severe noise, as long as the curve behaves as a centered ridge around that pixel. Assuming that the window size w is sufficiently small for the curve to be straight within its support, we still need to make sure that the curve is centered. To devise a criterion that guarantees the reliability of our direction estimate, we compute the correlation between the image and a Gaussian ridge of width σ_c over the window w (typically, $\sigma_c = 1$ pixel):

$$\rho(x,y) = \iint I(x+u, y+v)\, e^{-\frac{(u\cos\hat{\theta} + v\sin\hat{\theta})^2}{2\sigma_c^2}}$$
$$\times w(|u+iv|)\, \mathrm{d}u\,\mathrm{d}v \quad (9)$$

where $\hat{\theta}$ denotes $\hat{\theta}(x,y)$. If the curve goes through the pixel at (x,y), we know that the estimation $\hat{\theta}$ is very accurate and so, that $\rho(x,y)$ should be significantly larger than when this is not the case.

4. EXPERIMENTS

We compared the proposed method with several widely used algorithms [10, 16, 9]. We chose to show comparison with the steerable filter introduced and implemented by [9], which is under the matched filtering framework and yields the highest directional selectivity among these existing algorithms. We
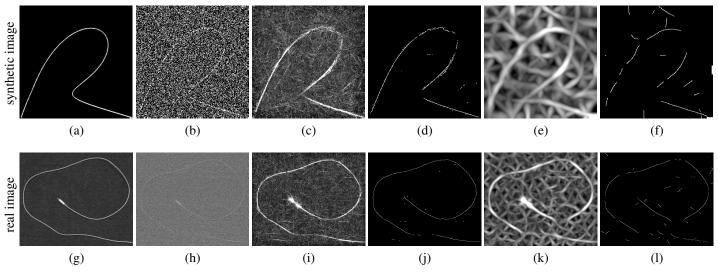
synthetic image					
(a)	(b)	(c)	(d)	(e)	(f)
real image					
(g)	(h)	(i)	(j)	(k)	(l)

Fig. 3. Curve detection from noisy images (in column 2, ground-truth in column 1): comparison of the results provided by our algorithm and the 4-th order steerable filter method [9]. Our algorithm: Column 3 shows the consistency map defined by (9) and column 4 shows the result of processing column 3 using non-maximum supression and thresholding; steerable filter algorithm: Column 5 shows the response map and column 6 shows the result of processing column 5 using the same non-maximum supression and thresholding.

chose the 4th-order filters for detecting ridges as suggested by the authors.

As for our algorithm, we chose the Gaussian window w to have a standard deviation $\sigma = 10$ pixels; we also used 20 moments and solved the maximization problem (7) by using a 360-point FFT.

We first generated a 256×256 synthetic curve image and added white Gaussian noise (Fig. 3 (a) and (b)). We also took a 467×567 photograph of a headphone cable under full and under weak light (Figs. 3 (g) and (h)). Figs. 3 (c) and (i) show the consistency map $\rho(x, y)$ defined by (9). Compared with the response map (Fig. 3 (e) and (k)) of the steerable filter method, the results of our algorithm show: 1) a more accurate localisation; and 2) much fewer ridge responses in non-ridge regions.

For both algorithms, we used the same non-maximum suppression and a thresholding that keeps a fixed number of pixels to get the final detection results (700 and 2000 for the synthetic image and the real image, respectively). Figs. 3 (d) and (j) show the final detection results of our algorithm, while Figs. 3 (f) and (l) show the results of the steerable filter method. These examples show that our algorithm produces less spurious ridges overall than the steerable filter method.

We conducted quantitative evaluation on the accuracy of both algorithms. We consider a pixel to be on a (continuously defined) curve if the distance from the pixel to the curve is less than 0.5 pixels. Then we define the detection rate of a detector as the number of pixels on the curve that are correctly identified by the detector, divided by the total number of pixels on the curve, i.e., the number of true positives over the total number of pixels on the curve. The first row in Table 1 shows that our method has a much higher detection rate. We

Table 1. Estimation error of curve location and direction.

Method	Fourier-Argand	Steerable Filter[9]
Detection Rate	54.89%	16.45%
Median Location Error	0.53 pixels	2.15 pixels
Mean Location Error	2.41 pixels	14.90 pixels
Median Direction Error	0.90 degrees	41.80 degrees
Mean Direction Error	1.94 degrees	35.57 degrees

also observe that, although many of the pixels detected by our method are not exactly on the curve, they are yet fairly close. This is confirmed by the computation of the median and the mean of the distances from the detected pixels to the curve. The results are listed in the 2nd and the 3rd rows of Table 1, and they show, again, that our method exhibits a significantly higher localization accuracy. Finally, a quantitative analysis of the accuracy of the estimated direction is shown in the last two rows of Table 1, and shows that our method provides the direction of the curve with significantly higher accuracy.

5. CONCLUSION

In this paper, we proposed a new approach for the detection of smooth curves from very noisy images. Specifically, we proposed to compute rotationally covariant moments (Fourier-Argand), and use a frequency estimation approach to retrieve the curve direction. We emphasize here that it is the collection of a sequence of such moments that allow us to estimate the direction with a high accuracy and very high robustness to noise. We also proposed a direction consistency criterion to distinguish curve from non-curve pixels. The proposed method is demonstrated by numerical experiments on both synthetic and real images.

6. REFERENCES

[1] Ahmed Kirmani, Dheera Venkatraman, Dongeek Shin, Andrea Colaço, Franco NC Wong, Jeffrey H Shapiro, and Vivek K Goyal, "First-photon imaging," *Science*, vol. 343, no. 6166, pp. 58–61, 2014.

[2] Genevieve Gariepy, Nikola Krstajić, Robert Henderson, Chunyong Li, Robert R Thomson, Gerald S Buller, Barmak Heshmat, Ramesh Raskar, Jonathan Leach, and Daniele Faccio, "Single-photon sensitive light-in-fight imaging," *Nature communications*, vol. 6, pp. 6021, 2015.

[3] Pablo Arbelaez, Michael Maire, Charless Fowlkes, and Jitendra Malik, "Contour detection and hierarchical image segmentation," *IEEE transactions on pattern analysis and machine intelligence*, vol. 33, no. 5, pp. 898–916, 2011.

[4] Joes Staal, Michael D Abràmoff, Meindert Niemeijer, Max A Viergever, and Bram Van Ginneken, "Ridge-based vessel segmentation in color images of the retina," *IEEE transactions on medical imaging*, vol. 23, no. 4, pp. 501–509, 2004.

[5] Y-I Tian, Takeo Kanade, and Jeffrey F Cohn, "Recognizing action units for facial expression analysis," *IEEE Transactions on pattern analysis and machine intelligence*, vol. 23, no. 2, pp. 97–115, 2001.

[6] Boris Epshtein, Eyal Ofek, and Yonatan Wexler, "Detecting text in natural scenes with stroke width transform," in *Computer Vision and Pattern Recognition (CVPR), 2010 IEEE Conference on*. IEEE, 2010, pp. 2963–2970.

[7] C Lawrence Zitnick and Piotr Dollár, "Edge boxes: Locating object proposals from edges," in *European conference on computer vision*. Springer, 2014, pp. 391–405.

[8] John Canny, "A computational approach to edge detection," *IEEE Transactions on pattern analysis and machine intelligence*, , no. 6, pp. 679–698, 1986.

[9] Mathews Jacob and Michael Unser, "Design of steerable filters for feature detection using Canny-like criteria," *IEEE transactions on pattern analysis and machine intelligence*, vol. 26, no. 8, pp. 1007–1019, 2004.

[10] Tony Lindeberg, "Edge detection and ridge detection with automatic scale selection," *International journal of computer vision*, vol. 30, no. 2, pp. 117–156, 1998.

[11] Wikipedia contributors, "Jean-Robert Argand — Wikipedia, the free encyclopedia," 2018, [Online; accessed 8-February-2019].

[12] Jean-Marc Lévy-Leblond, "If Fourier had known Argand... A geometrical point of view on Fourier transforms," *The Mathematical Intelligencer*, vol. 19, no. 4, pp. 63–71, 1997.

[13] B. Forster, T. Blu, D. Van De Ville, and M. Unser, "Shift-invariant spaces from rotation-covariant functions," *Applied and Computational Harmonic Analysis*, vol. 25, no. 2, pp. 240–265, September 2008.

[14] Michael Unser and Dimitri Van De Ville, "Wavelet steerability and the higher-order Riesz transform," *IEEE Transactions on Image Processing*, vol. 19, no. 3, pp. 636–652, 2010.

[15] T. Blu, P.-L. Dragotti, M. Vetterli, P. Marziliano, and L. Coulot, "Sparse sampling of signal innovations," *IEEE Signal Processing Magazine*, vol. 25, no. 2, pp. 31–40, March 2008.

[16] Antonio M López, Felipe Lumbreras, Joan Serrat, and Juan J. Villanueva, "Evaluation of methods for ridge and valley detection," *IEEE Transactions on pattern analysis and machine intelligence*, vol. 21, no. 4, pp. 327–335, 1999.